Journal of Alzheimer's Disease 51 (2016) 1275–1289
DOI 10.3233/JAD-150827
IOS Press

Does Microglial Activation Influence Hippocampal Volume and Neuronal Function in Alzheimer's Disease and Parkinson's Disease Dementia?

Grazia D. Femminella[a,1], Siddharth Ninan[a,1], Rebecca Atkinson[a], Zhen Fan[a], David J. Brooks[a,b] and Paul Edison[a,*]
[a]*Neurology Imaging Unit, Imperial College London, London, UK*
[b]*Department of Nuclear Medicine, Aarhus University, Denmark*

Accepted 13 January 2016

Abstract.
Background: The influence of neuroinflammation on neuronal function and hippocampal atrophy in Alzheimer's disease (AD) and Parkinson's disease dementia (PDD) is still unclear.
Objectives: Here we investigated whether microglial activation measured by [^{11}C]PK11195 PET is associated with neuronal function measured by cerebral glucose metabolic rate (rCMRGlc) using FDG-PET and hippocampal volume measurements.
Methods: We enrolled 25 subjects (9 PDD, 8 AD, and 8 controls) who underwent PET scans with [^{11}C](R)PK11195, [^{18}F]FDG, and volumetric MRI scanning.
Results: SPM correlation analysis in AD and PDD showed a negative correlation between hippocampal volume and microglial activation within hippocampus or parahippocampus and with cortical and subcortical areas of projections from hippocampus, while there was a positive correlation between rCMRGlc in cortical and subcortical areas of projections from hippocampus and hippocampal volume. Hippocampal volume was significantly reduced in AD compared to controls but not in PDD.
Conclusions: These findings indicate that microglial activation inversely correlated with hippocampal volume and hippocampal rCMRGlc in neurodegenerative diseases with dementia, providing further evidence for the central role of microglial activation in neurodegenerative diseases.

Keywords: Alzheimer's disease, neuroinflammation, Parkinson's disease with dementia, PET, volumetric MRI

INTRODUCTION

The role of neuroinflammation in neurodegenerative disease is still debated. While we know neuroinflammation plays a significant role in neurodegenerative disorders such as Alzheimer's disease (AD) and Parkinson's disease dementia (PDD), whether neuroinflammation is associated with local and distant neuronal damage is still not being investigated. Microglial cells are the resident macrophages of the central nervous system (CNS); they represent around 10% of the CNS population and play a crucial role in first line of immune defense in case of any kind of brain injury. They have the capability to phagocyte toxic products, release cytotoxic

[1]These authors contributed equally to this work.

*Correspondence to: Dr. Paul Edison, MBBS, MRCP, PhD, FRCPI, Clinical Senior Lecturer, Neurology Imaging Unit, Imperial College London, 1st Floor, B Block, Hammersmith Hospital Campus, Du Cane Road, London, W12 0NN, UK. Tel.: +44 2083833725; Fax: +44 2033134320; E-mail: paul.edison@imperial.ac.uk.

factors, and can be antigen-presenting cells [1]. In absence of foreign stimuli, microglial cells are in a "resting" state, or inactivated; however, with ramified morphology, microglia can scan close regions and their environment without interfering with neurons and neuronal activities and can monitor the brain parenchyma every few hours. When activated, they go through morphological changes, converting their shape to an activated amoeboid and mobile one, able to reach the site of injury [2]. These cells can remain for a long time in the activated phenotype, releasing cytokines and neurotoxic agents that can worsen CNS damage [3]. The acute CNS inflammatory response to an injury mediated by microglia can be protective; however, chronic inflammatory activity can be self-sustaining beyond physiological usefulness resulting in damage to the affected tissues [4]. In AD, β-fibrils activate microglia, and it is supported by the presence of microglia around the plaques, while in PDD, activated microglia is associated with α-synuclein. Microglial activation, as visualized by PET scans using the radioligand [^{11}C](R)PK11195 that targets the translocator protein (TSPO), is present in patients with AD and PD [5, 6]. It has also been shown that there is a strong association with amyloid deposition in AD [7].

Cerebral glucose metabolic rate (rCMRGlc) measured by [^{18}F]FDG PET is measure of glucose utilization, and is suggested to be an indirect measure of synaptic function. Hippocampal atrophy is a characteristic feature of AD, and it is established that accelerated hippocampal atrophy is associated with disease progression [8]. The presence of hippocampal atrophy in PDD is more variable; some groups have reported hippocampal atrophy in PD at an early stage of the disease [9–12], while others were not able to replicate those findings [13]. Here, we hypothesized that regional and distant microglial activation is associated with hippocampal volume loss in subjects with AD and PDD, and this could be associated with reduction in rCMRGlc. Our aim was to investigate whether increased hippocampal, medial temporal lobe, or whole cortex glial activation, where hippocampal neurons projects directly or indirectly, correlates with hippocampal volume loss and reduction in glucose metabolism in hippocampus and medial temporal lobe structures. In this study, we evaluated glial activation using [^{11}C]PK11195 PET and rCMRGlc using [^{18}F]FDG PET with arterial input. Hippocampal volume was measured from T1 volumetric MRI in patients with AD, PDD and age-matched control subjects.

MATERIALS AND METHODS

Study population

Twenty-five subjects (nine PDD, eight AD, and eight controls) were recruited from Imperial College London Healthcare NHS Trust and associated hospitals in London. All subjects had detailed clinical and neurological assessments, including collateral history as required, bloods and detailed neuropsychometric evaluation, assessing verbal and visual memory, attention, executive functions, visuoconstruction, language, and recognition memory. Subjects were diagnosed as clinically probable AD based on the NINDS-ADRDA criteria [14]. Diagnosis of PDD was based on the diagnostic algorithm for PDD [15], where patients had a diagnosis of PD for at least 1 year before the onset of dementia. The inclusion criteria for patients were: (1) age 50–80 years, (2) clinical diagnosis of AD or PDD before they enrolled in the study, (3) adequate visual and auditory acuity to complete the neuropsychometric testing, (4) a reliable caregiver who could provide information about the patient's clinical symptoms, and (5) ability to provide informed consent. Exclusion criteria were the presence of: (1) extensive white matter microvascular disease on MRI which was over and above the lacunes associated with normal aging, (2) major depression based on DSM-IV criteria, (3) a current or recent history of drug or alcohol abuse/dependence, (4) any significant disease or unstable medical condition that could influence neuropsychological testing, (5) pregnancy, (6) any contraindications to MRI, (7) a history of schizophrenia, schizoaffective disorder, bipolar disorder, or any history of electroconvulsive therapy, and (8) history of cancer within the past 5 years except localized skin and prostate cancer. Dementia was excluded in control subjects by detailed clinical examination and neuropsychometric tests. None of the enrolled subjects had diabetes or chronic kidney disease stage 3 and above. Two AD and one PDD subjects suffered from ischemic heart disease. None of the enrolled volunteers was on treatment for acute or chronic systemic inflammatory diseases. All patients underwent PET scans with [^{11}C]PK11195 PET and [^{18}F]FDG PET with arterial input as well as volumetric MRI scanning, after obtaining regulatory approval from the Ethics Committee of the Hammersmith Hospitals NHS Trust. Permission to administer radiotracers was obtained from the Administration of Radioactive Substances Advisory Committee (ARSAC), UK. The work described has been carried out in accordance

with The Code of Ethics of the World Medical Association (Declaration of Helsinki) and written informed consent was obtained by all participants. All subjects were age-matched AD and PDD subjects under 80 years.

MRI and PET scanning

MRI scanning

MRI scans were performed with a 1.5 Tesla GE scanner. T1 volumetric MRI (3D T1 volume, pulse sequence RF-Fast, acquisition times TR 30 ms, TE 3 ms, flip angle 30°, FOV 25 cm, matrix 156 × 256, voxel dimensions 0.98 × 0.98 × 1.6 mm) were acquired for co-registration of PET scans and assessment of atrophy, while T2 weighted images were acquired to rule out any structural abnormality in AD, PDD, and control subjects.

Evaluation of hippocampal volume using FreeSurfer

Automated hippocampal segmentation was done using FreeSurfer5.1.0 (http://surfer.nmr.mgh.harvard.edu/). The stages of FreeSurfer's volume-based subcortical stream are as fully described before [16, 17]. Briefly, an affine registration with Talairach space is followed by an initial volumetric labeling and correction for variation in intensity due to the B1 biasfield. After this, a high dimensional nonlinear volumetric alignment to the Talairach atlas is performed, followed by pre-processing, and finally the volume is labeled. Hippocampal volume was calculated by multiplying the number of voxels by the voxel volume.

PET scanning

[^{11}C](R)PK11195 PET. All subjects underwent three-dimensional [^{11}C](R)PK11195 PET using an ECAT EXACT HR++ (CTI/Siemens 966) scanner where a mean dose of 296(±18) MBq was injected, and 3D emission data was acquired in listmode over 60 min. Parametric images of [^{11}C](R)PK11195 binding potential (BP_{ND}), reflecting Bmax/Kd, were generated with a simplified tissue reference two brain compartmental model (SRTM). As AD and PDD subjects have a widespread distribution of pathological changes, no single region free of disease can be identified as a reference for non-specific tracer binding. This is due to the fact that (1) immunocytochemical study indicated TSPO is present in the cerebellum [18]; (2) TSPO is also present in arteries, meninges, choroid plexus, and in the ependymal cells, thus specific signal could be affected by the anatomical reference region even in healthy control subjects; and (3) with arterial input analysis, we have demonstrated that there is signal in cerebellum in AD subjects. Cluster analysis was, therefore, used to extract and identify a distributed cluster of voxels that mirrored a normal population cortical reference input function for each individual subject (controls, AD, and PDD). We have introduced this computational methodology that enables the extraction of a reference cluster from [^{11}C](R)PK11195 dynamic PET studies [18]. The algorithm matches the time activity curve (TAC) of each pixel to the kinetics of six pre-defined tissues (normal grey and normal white matter, skull, muscle, grey matter with reactive microglia, vasculature that is rich in the receptor in endothelial cells and smooth muscles) obtained from a database of control subjects and patients. The reference TAC is calculated as the population average of normal grey matter. The clustering code is implemented in the software package SUPERPK (Imperial Innovations, Imperial College London) written in Matlab (The Mathworks Inc., Natick MA). The use of an appropriate reference not only increases the sensitivity of the quantification procedure to the specific signal from microglia but also minimizes the sensitivity of the calculated binding potential (BP_{ND}), obtained by the modeling procedure, to changes in blood flow. Our unit has validated the use of the SRTM with a reference input function defined by cluster analysis as the most reproducible and sensitive technique for generating BP_{ND} maps [19].

[^{18}F]FDG-PET. All subjects underwent [^{18}F]FDG-PET scans using a Siemens ECAT EXACT HR+ scanner. Subjects were asked to fast for 4 h before the injection of [^{18}F]FDG (186 ± 8 MBq). The FDG dynamic emission scan was acquired over 60 min with continuous online whole blood sampling for the first 15 min while discrete whole blood and plasma samples were taken at 5, 10, 15, 20, 30, 40, 50, and 60 min. All subjects had radial artery cannulation and fasting plasma glucose levels were measured at the beginning and end of the scan. Parametric maps of absolute rCMRGlc were created by applying spectral analysis to brain time activity curves using an arterial plasma input function [7].

Region of interest analysis

Region of interest (ROI) analysis was done for parametric images of [^{11}C](R)PK11195 BP_{ND} and

rCMRGlc. Initially, an individualized object map was created for all the subjects using the following procedure. Statistical parametric mapping software (SPM8) was used to spatially transform individual PET images into their corresponding MRI space by: (1) segmenting individual MRIs into grey matter, white matter and CSF, (2) thresholding voxels with a >50% probability of containing grey matter to create individual grey matter binarized images, (3) transforming the probabilistic atlas in standard MNI space into the individual's MRI space, and (4) co-registering individual PET onto the corresponding MRI. The grey matter binarized image was then convolved with the atlas in Analyze 11 to create an individualized object map. Parametric images were then sampled for different cortical and subcortical regions.

Statistical parametric mapping (SPM) analysis

SPM interrogation to localize mean differences between patients and controls for [^{11}C](R)PK11195 BP_{ND} and rCMRGlc in AD and PDD was performed using SPM8 (Wellcome Department of Imaging Neuroscience, UCL, London, UK; http:www.fil.ion.ucl.ac.uk/spm). The between-group comparison was performed at a voxel level with a statistical threshold for significance set at $p < 0.01$ and an extent threshold of 50 voxels, as previously described [20]. All clusters with a corrected $p < 0.05$ were considered to be significant.

Statistical analysis

As hippocampal neurons project to the entorhinal cortex, which in turn projects to the whole of cortex, we anticipate that neuronal degeneration by microglial activation follows the cortical connection from hippocampus. Thus, to evaluate the relationship between hippocampal volume and neuroinflammation in AD and PDD subjects, pixel-by-pixel correlation between microglial activation, rCMRGlc and hippocampal volumes was evaluated using SPM where pixel-wise BP_{ND} of [^{11}C](R)PK11195 PET and rCMRGlc were the dependent variable and the hippocampal volume scores or hippocampal rCMRGlc were the covariate of interest.

Statistical analysis was performed using IBM SPSS 22 in Windows 7 (SPSS, Chicago, Illinois, USA). Continuous variables were expressed as mean ± SD. Normality was assessed using the Kolmogorov-Smirnov test. One-way ANOVA was used to compare the three groups followed by Bonferroni *post hoc* correction. The statistical interrogations of the ROI data for glial activation and glucose metabolism between AD and PDD versus controls was done with two-tailed *t*-test in SPSS22 with a significance of $p < 0.05$. We evaluated the major cortical regions like frontal lobe, temporal lobe, parietal lobe and occipital lobe. As medial temporal lobe and hippocampus are specifically involved in memory and neuroinflammation, we did a detailed analysis of medial temporal lobe and hippocampus. As anterior and posterior cingulate are implicated in amyloid deposition and reduction in glucose metabolism respectively, we subsequently analyzed anterior cingulate, posterior cingulate, thalamus and striatum. Categorical variables were compared by χ^2 test.

We have evaluated hippocampal volumetric measurements against [^{11}C](R)PK11195BP_{ND} and rCMRGlc in hippocampus, medial temporal lobe, and whole cortex and Spearman's correlation was employed by virtue of the limited sample size, and a $p < 0.05$ was considered as statistically significant. Correlations between Mini-Mental State Examination (MMSE) scores, [^{11}C](R)PK11195 BP_{ND}, rCMRGlc, and hippocampal volume were analyzed with Spearman's correlation and a $p < 0.05$ was considered as statistically significant.

RESULTS

Patient demographics

A total of 25 subjects (8 healthy controls, 8 AD, and 9 PDD) took part in the study. The mean age

Table 1
Demographic characteristics and neuropsychometric tests in control, AD, and PDD subjects

	Controls	AD	PDD
Total number	8	8	9
Mean Age (SD)	65.9 (6.2)	66.2 (6.4)	69.3 (4.1)
Age range	56–77	52–74	64–79
Gender (male)	6/8	5/8	5/9
MMSE (SD)	29.4 (0.9)	19 (5.3)*	21.3 (2.8)*
MMSE range	28–30	11–26	18–25
Immediate Word Recall (/10)	8.2 (0.7)	2.3 (1.0)*†	5.3 (0.9)*
Delayed Word Recall (/10)	7.9 (1.0)	0.6 (1.5)*†	6.0 (1.1)
Word Recognition	19.5 (0.8)	16.0 (1.7)*	16.7 (2.4)*
Forward Digit Span (/14)	13.4 (0.9)	5.5 (2.3)*	3.9 (2.2)*
Clock Drawing (/5)	4.9 (0.4)	1.3 (1.8)*	2.4 (1.5)*
Boston Naming Test (/30)	28.2 (1.0)	15.0 (4.2)*	21.0 (1.8)*
FAS	46.8 (2.1)	21.0 (12.8)*	20.1 (5.5)*

Data are presented as mean (SD). One way ANOVA and Chi-square test p values <0.05 are considered significant $^*p < 0.05$ versus Controls in pairwise comparisons; $^\dagger p < 0.05$ AD versus PDD in pairwise comparisons.

was 65.9 (±6.2) for controls, 66.2 (±6.4) for AD, and 69.3 (±4.1) for PDD, with no significant difference between the groups ($p = 0.253$). The mean MMSE scores were significantly different among the groups ($p < 0.001$), with pairwise comparisons showing no significant differences between AD (MMSE = 19 ± 5.3) and PDD (MMSE = 21.3 ± 2.8) ($p = 0.534$) and significant differences between AD and controls (MMSE = 29.4 ± 0.9) ($p < 0.001$) and PDD and controls ($p < 0.001$) (detailed characteristics are shown in Table 1). The neuropsychometric assessment revealed global deficits in short and long term memory, attention, constructional praxis, language, and recognition in both AD and PDD groups, with AD subjects showing significantly worse scores in short and long term memory compared to the PDD group (Table 1).

Voxel-level correlation between [^{11}C](R)PK11195 BP_{ND}, rCMRGlc, and hippocampal volume using SPM

To evaluate the relationship between hippocampal volume, microglial activation, and glucose metabolism, SPM pixel-by-pixel analysis was used in AD and PDD. In AD subjects, the biggest clusters of correlation between microglial activation and hippocampal volume involved the temporal, frontal, parietal, and occipital cortex, as well as hippocampus and parahippocampus; in PDD the clusters included amygdala and parahippocampus, as well as frontal, temporal, and occipital cortex. Figure 1A and B show significant clusters of microglial activation using multiple regression analysis of [^{11}C](R)PK11195 BP_{ND} against hippocampal volume in AD (A) and

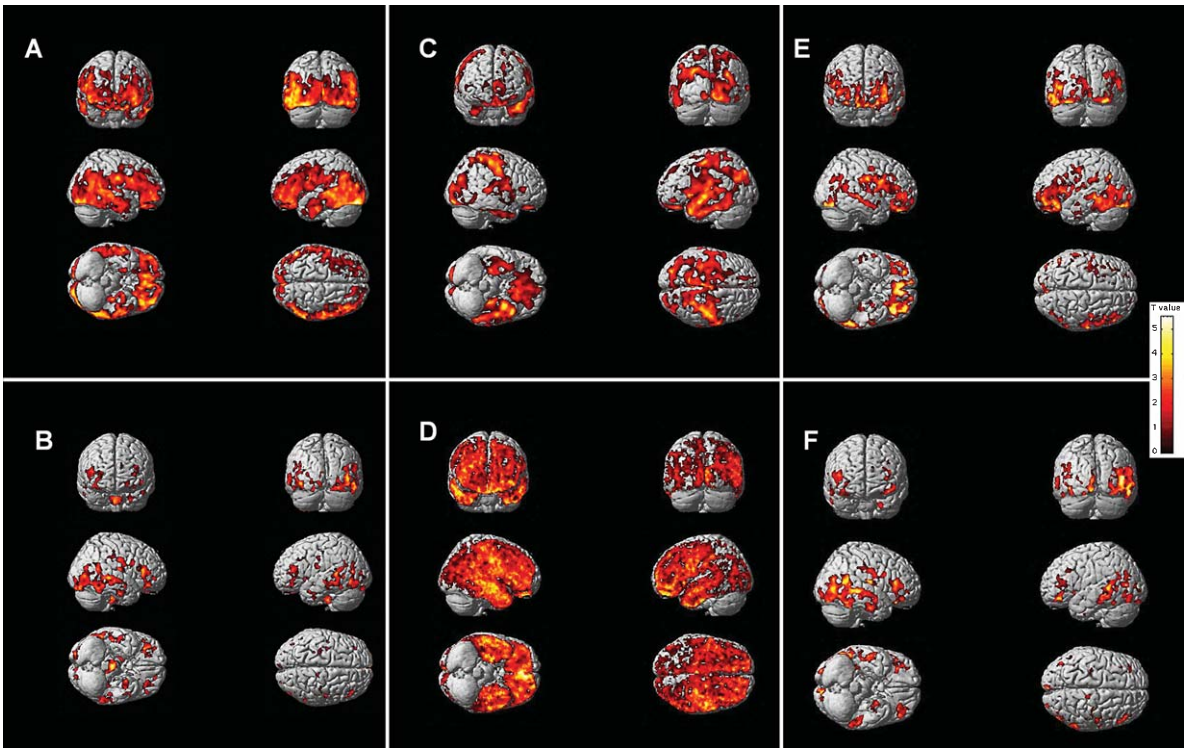

Fig. 1. Voxel-wise correlation between [^{11}C](R)PK11195BP_{ND} and hippocampal volume, between [^{11}C](R)PK11195 BP_{ND} and hippocampal rCMRGlc and between rCMRGlc and hippocampal volume in AD and PDD. Figure 1 represents voxel-wise relationship between levels of microglial activation and hippocampal volume by color-coded statistical parametric maps superimposed onto a spatially normalized MRI template image in AD (A) and PDD (B); Table 1 details corresponding significant clusters. Voxel-wise relationship between hippocampal glucose metabolism and levels of microglial activation is represented by color-coded statistical parametric maps superimposed onto a spatially normalized MRI template image in AD (C) and PDD (D); Table 2 details corresponding significant clusters. Voxel-wise relationship between glucose metabolism and hippocampal volume is represented by color-coded statistical parametric maps superimposed onto a spatially normalized MRI template image in AD (E) and PDD (F); Table 3 details corresponding significant clusters.

PDD (B) at a cluster threshold of $p < 0.00005$ with extent threshold of 200 voxels, where microglial activation was inversely correlated with hippocampal volume in AD and PDD subjects. Details of the cortical regions with [^{11}C](R)PK11195 BP_{ND} inversely associated with hippocampal volume in AD and PDD are shown in Table 2. Supplementary Figure 1 shows the clusters of significant [^{11}C](R)PK11195 uptake in AD and PDD subjects compared to controls.

Figure 1C and D shows significant clusters of increased [^{11}C](R)PK11195 BP_{ND} against hippocampal rCMRGlc in AD and PDD using multiple regression at a cluster threshold of $p < 0.000005$ for AD and $p < 0.00005$ for PDD with extent threshold of 200 voxels. In this case, an inverse correlation is observed between hippocampal glucose metabolism and cortical glial activation in AD and PDD subjects. Details of the cortical regions with hippocampal rCMRGlc inversely associated with [^{11}C](R)PK11195 BP_{ND} in AD and PDD are shown in Table 3. The clusters of significant correlation mainly involve frontal, temporal, and parietal cortex in AD subjects and frontal, temporal, and occipital cortex in PDD subjects.

Figure 1E and F shows the significant clusters of reduced rCMRGlc against hippocampal volume in AD (C) and PDD (D), with regression analysis at a cluster threshold of $p < 0.000005$ with extent threshold of 200 voxels. In this case, a direct correlation is observed between glucose metabolism and hippocampal volume in AD and PDD subjects. Details of the cortical regions with rCMRGlc inversely associated with hippocampal volume in AD and PDD are shown in Table 4, with significant clusters involving the temporal and occipital cortex in AD and the thalamus and temporal cortex in PDD.

Hippocampal volume, [^{11}C](R)PK11195BP_{ND}, and rCMRGlc in AD and PDD

The mean hippocampal total volume (left + right) was 8465.7 ± 639.2 mm^3 in control subjects, 6205.9 ± 1425.9 mm^3 in AD and 7568.7 ± 1095.4 mm^3 in PDD, indicating that hippocampal volume was significantly reduced in AD compared to controls ($p = 0.001$), while it was not significantly different in PDD subjects compared to controls ($p = 0.324$) at pairwise comparisons.

Table 5 shows [^{11}C](R)PK11195BP_{ND}in AD and PDD at ROI level compared to controls. [^{11}C](R)PK11195 BP_{ND} was significantly increased in all cortical ROIs in AD subjects compared to controls. Similarly, PDD subjects showed increased levels of microglial activation compared to controls in all cortical ROIs.

The regional cortical rCMRGlc in all groups is given in Table 5. PDD subjects showed significant reduction in glucose metabolism compared with the control subjects across all the regions; AD subjects showed reduced rCMRGlc compared to controls in all brain regions with the exception of anterior cingulate.

ROI correlation between [^{11}C](R)PK11195 BP_{ND}, rCMRGlc, and hippocampal volume

We have evaluated the correlation between hippocampal volume and levels of microglial activation and glucose metabolism in hippocampus in AD and PDD patients. Bias corrected and accelerated bootstrap 95% CIs are reported in square brackets. A significant inverse correlations between hippocampal volume and hippocampal glial activation was found, rho = –0.647 [–0.181, –0.893] ($p = 0.005$), as also reported in Fig. 3. When AD and PDD were analyzed separately, no significant correlations were found between hippocampal volume and [^{11}C](R)PK11195 BP_{ND} in hippocampus, medial temporal lobe, and the whole cortex at ROI levels. Hippocampal volume did not show significant correlations with rCMRGlc in hippocampus and medial temporal lobe in AD and PDD.

Correlation between Cognition, [^{11}C](R)PK11195 BP_{ND}, rCMRGlc, and hippocampal volume

In the present study we found significant correlations between MMSE and [^{11}C](R)PK11195 BP_{ND} in our predefined ROIs in the whole study population. In particular, MMSE was negatively correlated with [^{11}C](R)PK11195 BP_{ND} in hippocampus, rho = –0.483 [–0.700, –0.086] ($p = 0.029$), in the medial temporal lobe, rho = –0.585 [–0.801, –0.241] ($p = 0.002$) and in the whole cortex, rho = –0.632 [–0.836, –0.311] ($p = 0.001$).

Additionally, we have evaluated the relationship between cognitive function and hippocampal volume, finding a significant positive correlation between MMSE and hippocampal volume in the whole study group, rho = 0.505 [0.118, 0.786] ($p < 0.01$). MMSE also correlated with rCMRGlc in hippocampus, rho = 0.713 [0.457, 0.873] ($p < 0.0001$) and in the medial temporal lobe, rho = 0.678 [0.425, 0.834] ($p < 0.0001$).

Table 2
Clusters of voxel-by-voxel negative correlation between microglial activation and hippocampal volume in AD and PDD subjects using statistical parametric mapping

Region	Coordinates			Z-Score	Corrected *p* value	Cluster size
	x	y	z			
Negative correlation between PK11195 and hippocampal volume in AD subjects						
Left Posterior temporal lobe	–51	–66	–1	5.18	<0.00001	
Left Middle frontal gyrus	–33	54	–5	5.16	<0.00001	
Right Postcentral gyrus	61	–15	29	5.12	<0.00001	
Left Superior temporal gyrus	–63	–28	0	5.07	<0.00001	
Left Lateral occipital lobe	–28	–79	–19	5.06	<0.00001	426848
Left Inferolateral parietal lobe	–53	–63	32	5.00	<0.00001	
Right Posterior temporal lobe	63	–46	13	5.00	<0.00001	
Right Pallidum	15	0	–5	5.00	<0.00001	
Right Parahippocampal and ambient gyri	21	–1	–35	4.95	1.96268E-09	1487
Right Hippocampus	22	–6	–27	4.39	1.96268E-09	
Right Middle and inferior temporal gyrus	47	–4	–43	4.08	0.030565864	204
Right Anterior temporal lobe	42	2	–46	4.05	0.030565864	
Negative correlation between PK11195 and hippocampal volume in PDD subjects						
Left thalamus	–11	–21	0	4.88	2.7684E-08	2108
Brainstem	–10	–28	–8	4.32	2.7684E-08	
Pons	1	–25	–42	4.82	<0.00001	13120
Right thalamus	15	–25	–6	4.64	<0.00001	
Left Amygdala	–29	–2	–22	4.71	<0.00001	
Left Insula	–34	2	–11	4.61	<0.00001	
Left Middlle frontal gyrus	–33	36	11	4.56	<0.00001	
Left Inferior frontal gyrus	–35	32	6	4.49	<0.00001	
Left Putamen	–28	–7	0	4.39	<0.00001	14617
Left Anterior temporal lobe	–26	–1	–40	4.34	<0.00001	
Left Fusiform gyrus	–35	–5	–35	4.32	<0.00001	
Left Parahippocampal and ambient gyri	–26	–2	–33	4.27	<0.00001	
Right Lateral orbital gyrus	37	39	–12	4.68	<0.00001	
Right Inferior frontal gyrus	44	32	14	4.68	<0.00001	
Right Posterior orbital gyrus	34	34	–13	4.56	<0.00001	6571
Right Middlle frontal gyrus	27	46	4	4.33	<0.00001	
Right Insula	31	27	–2	4.15	<0.00001	
Right Posterior temporal lobe	53	–36	3	4.66	<0.00001	18550
Right Lateral occipital lobe	45	–77	1	4.50	<0.00001	
Right Superior temporal gyrus	56	–29	0	4.44	<0.00001	
Right Middle and inferior temporal gyrus	48	–15	–23	4.42	<0.00001	
Left Lingual gyrus	–9	–77	–11	4.61	0.002314216	557
Left Lateral occipital lobe	–40	–79	–9	4.49	1.12343E-12	3969
Left Posterior temporal lobe	–50	–66	–10	4.11	1.12343E-12	
Left Anterior orbital gyrus	–21	51	–9	4.47	0.017214791	359
Left Middle and inferior temporal gyrus	–50	–31	–12	4.36	<0.00001	6448
Left Inferiolateral parietal lobe	–52	–50	18	4.19	<0.00001	
Right Putamen	21	9	–5	4.43	1.04388E-07	1894
Right Insula	33	2	–8	4.18	1.04388E-07	
Right Postcentral gyrus	56	–14	17	4.39	4.996E-14	4616
Right Precentral gyrus	48	–10	33	4.35	4.996E-14	
Right Inferiolateral parietal lobe	48	–23	38	4.21	4.996E-14	
Right Lingual gyrus	12	–71	–10	4.37	2.92312E-05	1076
Left Precentral gyrus	–30	–24	54	4.33	0.003083954	527
Left Postcentral gyrus	–28	–34	57	4.16	0.003083954	
Left Anterior temporal lobe	–49	5	–26	4.08	0.006956356	445
Left Superior temporal gyrus	–45	11	–25	4.00	0.006956356	
Left Superior frontal gyrus	–7	47	17	4.17	0.007706112	435

Table 3
Clusters of voxel-by-voxel negative correlation between hippocampal glucose metabolism and microglial activation in AD and PDD subjects using statistical parametric mapping

Region	Coordinates			Z-Score	Corrected *p* value	Cluster size
	x	y	z			
Negative correlation between hippocampal rCMRGlc and PK11195 in AD subjects						
Left Lateral orbital gyrus	–39	33	–13	5.34	<0.00001	46847
Left Middle frontal gyrus	–32	54	–6	5.34	<0.00001	
Left Amygdala	–29	–5	–19	5.32	<0.00001	
Left Medial orbital gyrus	–15	29	–27	5.27	<0.00001	
Left Posterior orbital gyrus	–26	8	–16	5.18	<0.00001	
Left Superior frontal gyrus	–4	40	–16	5.17	<0.00001	
Left Putamen	–29	3	1	5.17	<0.00001	
Left Thalamus	–22	–31	1	5.14	<0.00001	
Left Pre-subgenual frontal cortex	–11	41	–5	5.14	<0.00001	
Right Straight gyrus	9	39	–22	5.13	<0.00001	
Left Straight gyrus	–3	36	–17	5.11	<0.00001	
Right Superior frontal gyrus	6	32	–14	5.09	<0.00001	
Left Posterior temporal lobe	–60	–43	–12	5.30	<0.00001	19954
Left Lateral occipital lobe	–32	–81	–20	5.15	<0.00001	
Right Posterior orbital gyrus	31	35	–21	5.26	<0.00001	19022
Right Postcentral gyrus	60	–15	30	5.18	<0.00001	
Right Precentral gyrus	61	3	11	5.07	<0.00001	
Right Inferior frontal gyrus	46	12	27	5.01	<0.00001	
Right Lateral orbital gyrus	45	27	–15	5.01	<0.00001	
Right Middle frontal gyrus	45	16	34	5.00	<0.00001	
Right Anterior orbital gyrus	30	50	–8	4.92	<0.00001	
Right Lateral occipital lobe	33	–76	–17	5.25	<0.00001	19795
Right Middle and inferior temporal gyrus	50	–25	–5	5.24	<0.00001	
Right Posterior temporal lobe	60	–53	13	5.05	<0.00001	
Right Cuneus	–1	–81	14	5.04	<0.00001	
Left Lateral occipital lobe	–21	–79	26	5.02	<0.00001	
Right Lingual gyrus	18	–80	–15	4.99	<0.00001	
Right Superior temporal gyrus	56	6	–11	4.89	<0.00001	
Right Pallidum	14	–2	–7	5.08	5.75183E-09	345
Right Putamen	17	5	–8	4.70	5.75183E-09	
Right Thalamus	19	–25	4	5.08	<0.00001	1382
Left Inferiolateral parietal lobe	–62	–31	28	5.04	<0.00001	1127
Right Gyrus cinguli	4	–36	39	4.94	<0.00001	2005
Left Gyrus cinguli	–7	–40	41	4.78	<0.00001	
Right Superior parietal gyrus	14	–57	17	4.65	<0.00001	
Left Precentral gyrus	–39	–10	47	4.90	<0.00001	3044
Right Postcentral gyrus	–62	–8	11	4.86	1.14353E-14	725
Left Cingulate gyrus	–10	24	26	4.80	5.81757E-14	673
Left Middle and inferior temporal gyrus	–58	–1	–31	4.77	9.21485E-15	732
Left Anterior temporal lobe	–61	4	–27	4.59	9.21485E-15	732
Right Insula	41	–5	1	4.63	1.84439E-08	316
Negative correlation between hippocampal rCMRGlc and PK11195 in PDD subjects						
Left Thalamus	–11	–20	1	5.05	4.82582E-06	1130
Left Cuneus	–1	–97	6	4.99	1.05693E-13	3776
Left Lingual gyrus	–9	–77	–10	4.96	1.05693E-13	
Right Posterior temporal lobe	53	–36	3	4.81	<0.00001	23424
Right Middle and inferior temporal gyrus	48	–14	–25	4.71	<0.00001	
Right Lateral occipital lobe	45	–75	3	4.70	<0.00001	
Right Thalamus	14	–23	–6	4.76	0.000367193	657
Right Postcentral gyrus	62	–10	15	4.75	1.55431E-15	4546
Right Inferior frontal gyrus	43	10	27	4.38	1.55431E-15	

(*Continued*)

Table 3
(*Continued*)

Negative correlation between hippocampal rCMRGlc and PK11195 in AD subjects						
Region	Coordinates			Z-Score	Corrected *p* value	Cluster size
	x	y	z			
Right Inferiolateral parietal lobe	48	–24	38	4.25	1.55431E-15	
Right Precentral gyrus	35	–20	52	4.17	1.55431E-15	
Left Posterior temporal lobe	–39	–66	10	4.54	1.93313E-08	1845
Left Lateral occipital lobe	–44	–74	10	4.38	1.93313E-08	
Right Posterior orbital gyrus	34	32	–17	4.53	3.72107E-06	1161
Right Lateral orbital gyrus	38	42	–13	4.52	3.72107E-06	
Left Middle and inferior temporal gyrus	–51	–32	–12	4.51	<0.00001	5406
Left Inferiolateral parietal lobe	–49	–59	22	4.18	<0.00001	
Left Insula	–33	3	–10	4.48	<0.00001	8439
Left Anterior orbital gyrus	–33	47	–18	4.45	<0.00001	
Left Lateral orbital gyrus	–40	44	–14	4.43	<0.00001	
Left Putamen	–27	–7	0	4.35	<0.00001	
Left Inferior frontal gyrus	–35	26	9	4.27	<0.00001	
Left Middle frontal gyrus	–35	38	8	4.24	<0.00001	
Right Putamen	22	9	–6	4.46	2.63261E-08	1802
Right Insula	32	2	–7	4.33	2.63261E-08	
Left Anterior temporal lobe	–24	–1	–38	4.42	4.20566E-05	883
Left Fusiform gyrus	–29	–4	–37	4.27	4.20566E-05	
Right Fusiform gyrus	35	–31	–22	4.17	0.025341649	285
Left Gyrus cinguli	–2	–48	21	4.29	0.007849918	378
Right Gyrus cinguli	1	–42	26	4.05	0.007849918	
Left Superior parietal gyrus	–2	–52	15	3.90	0.007849918	
Right Middle frontal gyrus	33	49	0	4.14	0.047104668	239

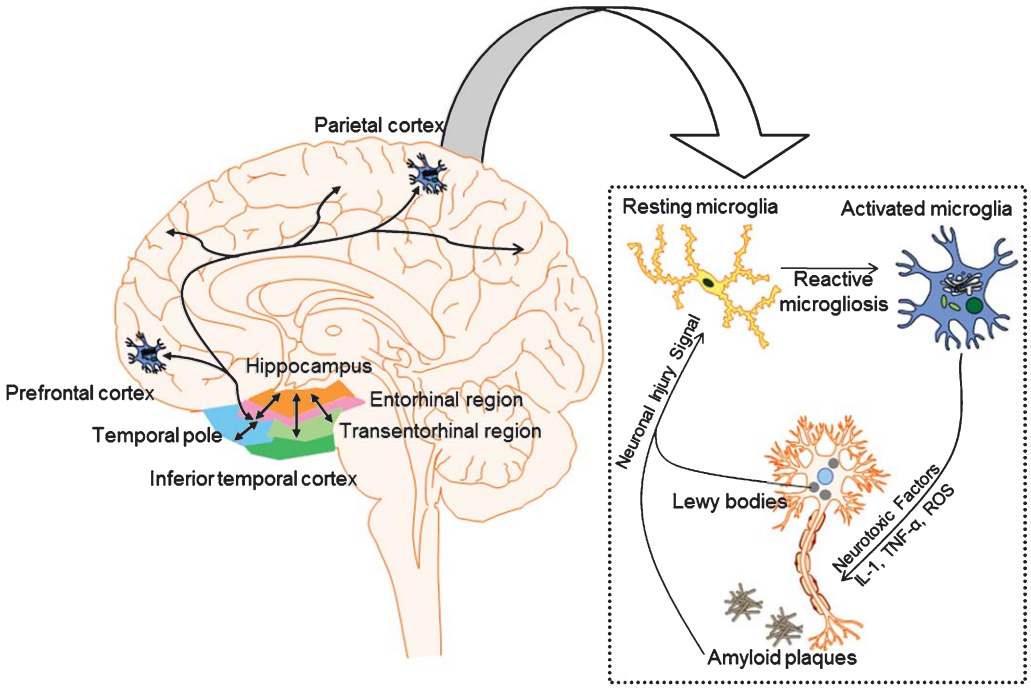

Fig. 2. Potential role of local and distant neuroinflammatory triggers on hippocampal neurodegeneration. Figure 2 left schematically represents hippocampal connections with entorhinal cortex and cerebral cortical regions. On the right, this figure shows how direct inflammatory triggers (amyloid plaques, Lewy bodies) can generate a vicious cycle of cytotoxic and stimulatory factors that leads to chronic neuroinflammation and progressive neuronal degeneration over time.

Table 4
Clusters of voxel-by-voxel positive correlation between brain glucose metabolism and hippocampal volume in AD and PDD subjects using statistical parametric mapping

Region	Coordinates			Z- Score	Corrected *p* value	Cluster size
	x	y	z			
Positive correlation between rCMRGlc and hippocampal volume in AD subjects						
Left Superior temporal gyrus	–47	–7	–12	6.36	<0.00001	
Left Nucleus accumbens	–6	5	–11	6.13	<0.00001	
Left thalamus	–20	–35	–2	6.10	<0.00001	
Left Superior parietal gyrus	–4	–67	18	6.04	<0.00001	
Right Lingual gyrus	11	–50	–2	6.01	<0.00001	
Left Posterior temporal lobe	–26	–35	–20	5.92	<0.00001	
Left Subcallosal area	–2	10	–10	5.92	<0.00001	
Left insula	–39	–10	–5	5.91	<0.00001	377553
Right Posterior temporal lobe	15	–35	–3	5.88	<0.00001	
Right Precentral gyrus	17	–18	71	5.87	<0.00001	
Left Lateral occipital lobe	–22	–84	40	5.81	<0.00001	
Right Lateral occipital lobe	19	–89	–14	5.80	<0.00001	
Left Anterior temporal lobe	–32	–1	–32	5.78	<0.00001	
Left Superior temporal gyrus	–43	14	–28	5.76	<0.00001	
Left Superior frontal gyrus	–14	45	45	4.89	1.56541E-14	1300
Right amygdala	26	–5	–15	4.84	3.30955E-05	251
Right Inferior frontal gyrus	49	28	9	4.74	1.15463E-13	1181
Right thalamus	16	–14	10	4.57	4.04715E-05	244
Positive correlation between rCMRGlc and hippocampal volume in PDD subjects						
Left Thalamus	–10	–18	–4	6.56	<0.00001	
Left Gyrus cinguli	–4	–44	28	6.45	<0.00001	
Right Precentral gyrus	20	–14	64	6.45	<0.00001	
Right Superior temporal gyrus	52	–6	–14	6.38	<0.00001	
Right Superior temporal gyrus	50	14	–24	6.34	<0.00001	
Right Thalamus	14	–16	2	6.33	<0.00001	79141
Right Postcentral gyrus	54	–12	36	6.32	<0.00001	
Right Lateral orbital gyrus	–44	40	–12	6.31	<0.00001	
Right Anterior orbital gyrus	18	50	–18	6.30	<0.00001	
Right Middle and inferior temporal gyrus	56	–8	–18	6.28	<0.00001	
Right Hippocampus	22	–12	–22	6.28	<0.00001	
Left Posterior temporal lobe	–32	–36	–20	6.26	<0.00001	
Left Gyrus cinguli	–2	–24	44	6.22	<0.00001	

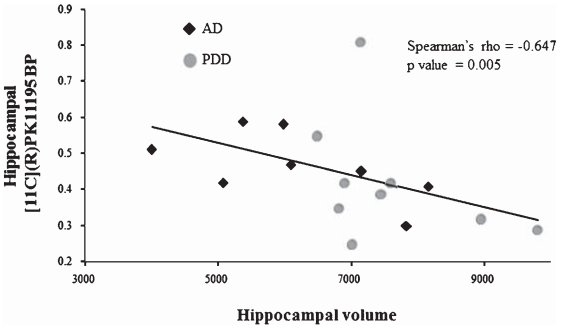

Fig. 3. Correlation between hippocampal volume and hippocampal microglial activation in AD and PDD.

DISCUSSION

In this study we have demonstrated for the first time that levels of microglial activation at voxel level in the whole cortex, medial temporal lobe and hippocampus, measured using [^{11}C](R)PK11195PET, were inversely correlated with hippocampal volume and hippocampal glucose uptake in AD and PDD subjects. This study provides further credence to the hypothesis that microglial activation detected with [^{11}C](R)PK11195 PET is correlated with markers of neuronal damage as reduction in hippocampal volume and glucose metabolism. This finding further supports the role of neuroinflammation and microglial activation in neurodegenerative diseases [5, 7, 20–22]. The spatial agreement between local and distant microglial activation in the cortical projections and atrophy in hippocampus lends credence to the theory that chronically activated microglial cells might be one of the effectors of neurodegenerative processes; thus, influencing neuroinflammation can have potential therapeutic implications in these diseases. In this study we have found increased levels of [^{11}C](R)PK11195 BP_{ND} across almost

Table 5
Regional microglial activation and glucose metabolism in control, AD, and PDD subjects

	Controls	AD	PDD
Regional microglial activation			
Hippocampus BP_{ND}	0.34 (0.09)	0.47 (0.09)*	0.42 (0.17)
Anterior Cingulate BP_{ND}	0.34 (0.09)	0.52 (0.17)*	0.49 (0.21)*
Posterior Cingulate BP_{ND}	0.40 (0.09)	0.60 (0.18)*	0.57 (0.22)*
Thalamus BP_{ND}	0.39 (0.13)	0.51 (0.10)*	0.54 (0.23)
Striatum BP_{ND}	0.26 (0.06)	0.44 (0.12)*	0.45 (0.16)*
Frontal lobe BP_{ND}	0.30 (0.10)	0.50 (0.10)*	0.46 (0.18)*
Temporal lobe BP_{ND}	0.33 (0.07)	0.48 (0.11)*	0.43 (0.13)*
Parietal lobe BP_{ND}	0.30 (0.10)	0.46 (0.11)*	0.43 (0.16)*
Occipital lobe BP_{ND}	0.36 (0.08)	0.52 (0.10)*	0.50 (0.15)*
Medial Temporal Lobe BP_{ND}	0.32 (0.08)	0.46 (0.11)*	0.45 (0.14)*
Cortical BP_{ND}	0.34 (0.08)	0.51 (0.12)*	0.47 (0.16)*
Regional glucose metabolism			
Hippocampus BP_{ND}	0.25 (0.02)	0.19 (0.02)*	0.21 (0.03)*
Anterior Cingulate BP_{ND}	0.30 (0.03)	0.28 (0.05)	0.26 (0.04)*
Posterior Cingulate BP_{ND}	0.37 (0.04)	0.28 (0.04)*	0.29 (0.03)*
Thalamus BP_{ND}	0.29 (0.05)	0.24 (0.04)*	0.23 (0.04)*
Striatum BP_{ND}	0.36 (0.04)	0.31 (0.05)*	0.29 (0.05)*
Frontal lobe BP_{ND}	0.34 (0.03)	0.29 (0.05)*	0.25 (0.04)*
Temporal lobe BP_{ND}	0.29 (0.03)	0.23 (0.04)*	0.21 (0.03)*
Parietal lobe BP_{ND}	0.34 (0.03)	0.26 (0.04)*	0.23 (0.04)*
Occipital lobe BP_{ND}	0.33 (0.02)	0.28 (0.06)*	0.22 (0.05)*
Medial Temporal Lobe BP_{ND}	0.23 (0.02)	0.18 (0.02)*	0.21 (0.03)*

Data are presented as mean (SD). *$p < 0.05$ versus controls.

all predefined brain regions in AD and PDD subjects compared to controls, consistent with previous reports.

Growing evidence indicates that neuroinflammation contributes significantly to the pathological process in chronic neurodegenerative diseases, and this could act independently and along with the other pathological substrates in neurodegenerative diseases. In AD, microglial cells are activated by amyloid deposition, generating a proinflammatory response leading to neuronal death. The damaged neurons and neurofibrillary tangles can in turn activate microglia, inducing a vicious cycle of neuronal damage and reactive gliosis [23]. In PD, findings from neuropathological studies have shown that microglial cells are associated with α-synuclein-positive Lewy neurites [24], and that misfolded α-synuclein released from neurons can directly activate microglial cells. In PDD, according to Braak and colleagues, the spread of Lewy body pathology starts from dorsal motor nucleus of vagus and olfactory nucleus, then reaches substantia nigra, basal forebrain, and ultimately the sensory association areas and premotor areas of the neocortex. Thus, it could be implied that neuroinflammation triggered by Lewy body pathology follows the same temporal-spatial progression, which in turn could lead to neuronal damage both in anterograde and retrograde fashion. Moreover, it has been demonstrated that microglial activation may lead to synaptic dysfunction and loss of dopaminergic axonal projections, with retrograde neurodegeneration [25, 26]. In this study we have shown that microglial activation locally and in the cortical projections from hippocampus, could cause neuronal damage and hippocampal atrophy, which is novel, and has never been demonstrated before.

It should also be mentioned that microglial cells in brain express different phenotypes, depending on the type of proinflammatory stimuli received, either via paracrine or autocrine manner [27]. The cytokine stimulation is essential for microglial polarization into the classically activated M1, or the M2 phenotype, which is activated by the alternate pathway [28]. In AD, it has also been demonstrated that dysfunctional microglial response could contribute to Aβ accumulation [29]. As AD pathology worsens, there is a switch from M2 to M1 phenotype consistent with the idea that microglia become less responsive to M2 induction signals as they age [30–32]. In our study, we cannot discern whether glial activation detected by [^{11}C](R)PK11195 PET might be mainly due to either of the two phenotypes. However, microglial activation detected by [^{11}C](R)PK11195 PET is associated with hippocampal volume loss and correlated with MMSE, suggesting the putative effect of the microglial cells as described before.

It is known that other factors can affect neuroinflammation, such as the activity of the central adrenergic system. As an example, multiple lines of evidence indicate that the adrenergic neurotransmitter norepinephrine also exerts anti-inflammatory actions within the CNS. In transgenic AD mouse models with locus coeruleus (the major source of noradrenergic projections) degeneration, the decrease of norepinephrine has shown to induce the inflammatory reaction of microglial cells in AD and to exacerbate neuroinflammation induced by the deposition of amyloid [33–35].

In this study, we have also demonstrated that hippocampal volume in AD and PDD subjects is directly correlated with reduction in glucose metabolism at voxel level. This finding is in accordance with previous evidence which have shown that patients with AD and PDD have extensive areas of cerebral atrophy and hypometabolism in comparison with control subjects. Vander Borght et al. compared AD and PDD subjects matched for dementia severity, finding similar metabolic reductions both globally and regionally; however, PDD exhibited greater metabolic reduction in the occipital cortex but relatively preserved metabolism in the medial temporal lobe compared to AD. FDG-PET studies in AD have indicated that glucose metabolic deficits start from the hippocampus and posterior cingulate cortex, and then involve the temporo-parietal cortices [36]. In this study we have been able to demonstrate a similar pattern of hypometabolism and increase in microglial activation on those regions.

Recent data have demonstrated that in PD patients with mild cognitive impairment, hypometabolism exceeds atrophy in the angular gyrus, occipital, orbital, and anterior frontal lobes [37]. In PDD patients, the hypometabolic areas observed in PD patients with mild cognitive impairment were replaced by areas of atrophy, which were surrounded by extensive zones of hypometabolism; areas where atrophy extended more than hypometabolism were found in the precentral and supplementary motor areas in both patients with mild cognitive impairment and with PDD, and in the hippocampus and temporal lobe in patients with PDD.

These data are also in accordance with our findings. First of all, while we found significant hippocampal atrophy in AD subjects, we were not able to detect any significant differences in hippocampal volume between PDD and controls. Previous reports evaluating hippocampal volume in PD and PDD patients showed conflicting results. Some authors have reported hippocampal atrophy even at early stages of the disease, while others have not found significant differences compared to age-matched controls [9–13]. Although mixed AD-PD pathology can be present in our study population, our PDD patients did not show significant hippocampal atrophy compared to age-matched controls. Our AD group also showed occipital hypometabolism which more commonly is observed in PDD; however, this finding has been observed in works from our studies and others [38–40]. Unlike other studies, our measurement of rCMRGlc was quantitative and absolute, as we used the arterial input for the FDG-PET scans.

We evaluated the correlation between microglial activation in the hippocampus, and cortical regions where death of neuronal projections (direct and indirect) from the hippocampus could influence the level of microglial activation due to the death of the neurons in the medial temporal lobe and neocortical regions, as microglial activation and neuronal death in the hippocampus could lead to microglial activation in the projected neurons. The hippocampal fibers are connected directly to the entorhinal cortex, and from there project on to perirhinal, parahippocampal cortices and widely to the cortex. This correlation suggests that microglial activation could cause neuronal damage in the immediate vicinity as well as at distant regions connected indirectly from the hippocampus. It is suggested that this could be due to the loss of afferent and efferent fibers from the hippocampal neurons, while cortical microglial activation independent of hippocampal denervation is also a possibility. This phenomenon is also reported in stroke [41].

Indeed, in our cohort hippocampal atrophy in AD group seems to correlate well with neuroinflammation within the hippocampus and in regions of direct or indirect cortical projections. It is known that enthorinal cortex within the medial temporal lobe is connected both via afferent and efferent neuronal pathways to hippocampus. Moreover, the enthorinal cortex is also connected to a variety of cortical and subcortical regions: amygdala, olfactory bulb, cingulate cortex, temporal cortex, and the orbital cortex (along with other frontal and parietal regions). Thus, it is conceivable that neuroinflammation in the hippocampus could lead to neuronal dysfunction locally and remotely in connected cortical areas, possibly leading to neurodegeneration and atrophy (Fig. 2). It could also be argued that microglial activation in cortical areas of hippocampal projection might lead to neuroinflammation and atrophy within the

hippocampus. It is likely that both these processes might happen in AD pathology, leading to a vicious cycle of neurodegeneration. Interestingly, our data set demonstrated that hippocampal volume correlated significantly to the reduction in rCMRGlc and to the increase in microglial activation in AD in wider (in terms of voxel volume) brain regions compared to PDD, suggesting that, for comparable cognitive status, the underlying microglial activation and reduction in rCMRGlc is spatially more widespread in AD than PDD, and accordingly significant atrophy has set in AD but not in PDD. Similarly, we have found that the reduction in hippocampal glucose metabolism in AD is associated with wider areas of increased glial activation compared to PDD. This could suggest that cognitive dysfunction in PDD is also contributed by other factors like presence of α-synuclein.

The neuropsychometric assessment of the study population indicated that the AD group achieved significantly lower scores than PDD in immediate and delayed memory recall. This is partially in accordance with previous studies that have shown that, for comparable MMSE levels, AD and PDD patients perform differently on memory, attention and executive functions, even at early stages of the disease [42, 43]. This could be due to the different neuropathological substrate, which in AD affects primarily the medial temporal cortex and the neocortical association areas, while in PD neurodegeneration starts in the brain stem and subsequently spreads to the cortical areas. In the present study we have also found significant negative correlations between cognitive profile as measured by MMSE scores versus [^{11}C](R)PK11195 BP_{ND}; and a positive correlation between MMSE score versus hippocampal volume, and MMSE scores versus rCMRGlc, further suggesting the putative effect of microglial activation in late stage of the disease [44, 45].

The findings of this study are limited by the small number of subjects per group and by the cross-sectional design, however, this proof of principle study sheds more light into the role of neuroinflammation, and how this influences the neurodegenerative process. Also, the use of multiple comparisons might increase the risk of false positive inferences (type I error); we have reduced this error by applying correction for multiple comparisons in our regression analysis. [^{11}C](R)PK11195 PET, though used for many years as a selective marker of microglial activation via binding to the upregulated TPSO protein, shows *in vivo* binding 1-2 orders of magnitude lower than second-generation TPSO tracers like [^{11}C]PBR28. It has been shown that the rate of clearance of [^{11}C](R)-PK11195 is considerably faster than many other widely used PET radioligands leading to a very low ratio of specific to non-specific binding. It is also suggested that the fraction of non-specifically bound [^{11}C](R)-PK11195 in the grey matter is about 60%. However, reproducibility studies with [^{11}C](R)-PK11195 have shown that the tracer binding in large brain regions was acceptable for applied clinical studies [46]. Future studies with second generation TSPO markers may be able to extend these results further in other neurodegenerative diseases. However, second-generation tracers are influenced by the TSPO polymorphism. Moreover, although [^{11}C](R)PK11195 is generally considered as a specific marker for activated microglial cells, several studies have suggested that this tracer also binds to reactive astrocytes in brain [47–49]. Another limitation of the present study is that the observed correlations between hippocampal volume and [^{11}C](R)PK11195 BP_{ND} at the ROI level, were not evident when the groups were analyzed separately. Although we cannot exclude that this is just simply attributable to differences between groups, there was no significant difference between microglial activation between these two groups. However, we were only able to evaluate small numbers of subjects, as enrolment of a larger number of subjects was limited by the intensity of scanning involved in this study. Previous reports from our group have shown that a correlation exists between MMSE scores and cortical microglial activation at a voxel level using SPM analysis both in AD subjects and PDD subjects separately [38].

In conclusion, we have shown that glial activation within the hippocampus, as assessed by [^{11}C](R)PK11195PET, inversely correlates with hippocampal volume in neurodegenerative diseases with dementia. These findings provide further evidence for the central role of microglial activation in neurodegenerative pathologies like AD and PDD, and highlights microglial activation as a potential therapeutic target in combating chronic neuroinflammation and resultant neurodegeneration.

ACKNOWLEDGMENTS

This work was supported by the Medical Research Council grant number G1100810, by the National Institute for Health Research (NIHR) Imperial Biomedical Research Centre and by the Alzheimer's Research UK.

Authors' disclosures available online (http://j-alz.com/manuscript-disclosures/15-0827r2).

SUPPLEMENTARY MATERIAL

The supplementary material is available in the electronic version of this article: http://dx.doi.org/10.3233/JAD-150827.

REFERENCES

[1] Morales I, Guzman-Martinez L, Cerda-Troncoso C, Farias GA, Maccioni RB (2014) Neuroinflammation in the pathogenesis of Alzheimer's disease. A rational framework for the search of novel therapeutic approaches. *Front Cell Neurosci* **8**, 112.

[2] Hanisch UK, Kettenmann H (2007) Microglia: Active sensor and versatile effector cells in the normal and pathologic brain. *Nat Neurosci* **10**, 1387-1394.

[3] Liu B, Hong JS (2003) Role of microglia in inflammation-mediated neurodegenerative diseases: Mechanisms and strategies for therapeutic intervention. *J Pharmacol Exp Ther* **304**, 1-7.

[4] Frank-Cannon TC, Alto LT, McAlpine FE, Tansey MG (2009) Does neuroinflammation fan the flame in neurodegenerative diseases? *Mol Neurodegener* **4**, 47.

[5] Edison P, Archer HA, Gerhard A, Hinz R, Pavese N, Turkheimer FE, Hammers A, Tai YF, Fox N, Kennedy A, Rossor M, Brooks DJ (2008) Microglia, amyloid, and cognition in Alzheimer's disease: An [11C](R)PK11195-PET and [11C]PIB-PET study. *Neurobiol Dis* **32**, 412-419.

[6] Cagnin A, Gerhard A, Banati RB (2002) *In vivo* imaging of neuroinflammation. *Eur Neuropsychopharmacol* **12**, 581-586.

[7] Edison P, Ahmed I, Fan Z, Hinz R, Gelosa G, Ray Chaudhuri K, Walker Z, Turkheimer FE, Brooks DJ (2013) Microglia, amyloid, and glucose metabolism in Parkinson's disease with and without dementia. *Neuropsychopharmacology* **38**, 938-949.

[8] Leung KK, Bartlett JW, Barnes J, Manning EN, Ourselin S, Fox NC, Alzheimer's Disease Neuroimaging Initiative (2013) Cerebral atrophy in mild cognitive impairment and Alzheimer disease: Rates and acceleration. *Neurology* **80**, 648-654.

[9] Melzer TR, Watts R, MacAskill MR, Pitcher TL, Livingston L, Keenan RJ, Dalrymple-Alford JC, Anderson TJ (2012) Grey matter atrophy in cognitively impaired Parkinson's disease. *J Neurol Neurosurg Psychiatry* **83**, 188-194.

[10] Beyer MK, Janvin CC, Larsen JP, Aarsland D (2007) A magnetic resonance imaging study of patients with Parkinson's disease with mild cognitive impairment and dementia using voxel-based morphometry. *J Neurol Neurosurg Psychiatry* **78**, 254-259.

[11] Camicioli R, Moore MM, Kinney A, Corbridge E, Glassberg K, Kaye JA (2003) Parkinson's disease is associated with hippocampal atrophy. *Mov Disord* **18**, 784-790.

[12] Laakso MP, Partanen K, Riekkinen P, Lehtovirta M, Helkala EL, Hallikainen M, Hanninen T, Vainio P, Soininen H (1996) Hippocampal volumes in Alzheimer's disease, Parkinson's disease with and without dementia, and in vascular dementia: An MRI study. *Neurology* **46**, 678-681.

[13] Apostolova LG, Beyer M, Green AE, Hwang KS, Morra JH, Chou YY, Avedissian C, Aarsland D, Janvin CC, Larsen JP, Cummings JL, Thompson PM (2010) Hippocampal, caudate, and ventricular changes in Parkinson's disease with and without dementia. *Mov Disord* **25**, 687-695.

[14] McKhann GM, Knopman DS, Chertkow H, Hyman BT, Jack CR Jr, Kawas CH, Klunk WE, Koroshetz WJ, Manly JJ, Mayeux R, Mohs RC, Morris JC, Rossor MN, Scheltens P, Carrillo MC, Thies B, Weintraub S, Phelps CH (2011) The diagnosis of dementia due to Alzheimer's disease: Recommendations from the National Institute on Aging-Alzheimer's Association workgroups on diagnostic guidelines for Alzheimer's disease. *Alzheimers Dement* **7**, 263-269.

[15] Emre M (2003) Dementia associated with Parkinson's disease. *Lancet Neurol* **2**, 229-237.

[16] Fischl B, van der Kouwe A, Destrieux C, Halgren E, Segonne F, Salat DH, Busa E, Seidman LJ, Goldstein J, Kennedy D, Caviness V, Makris N, Rosen B, Dale AM (2004) Automatically parcellating the human cerebral cortex. *Cereb Cortex* **14**, 11-22.

[17] Fischl B, Salat DH, Busa E, Albert M, Dieterich M, Haselgrove C, van der Kouwe A, Killiany R, Kennedy D, Klaveness S, Montillo A, Makris N, Rosen B, Dale AM (2002) Whole brain segmentation: Automated labeling of neuroanatomical structures in the human brain. *Neuron* **33**, 341-355.

[18] Turkheimer FE, Edison P, Pavese N, Roncaroli F, Anderson AN, Hammers A, Gerhard A, Hinz R, Tai YF, Brooks DJ (2007) Reference and target region modeling of [11C]-(R)-PK11195 brain studies. *J Nucl Med* **48**, 158-167.

[19] Anderson AN, Pavese N, Edison P, Tai YF, Hammers A, Gerhard A, Brooks DJ, Turkheimer FE (2007) A systematic comparison of kinetic modelling methods generating parametric maps for [(11)C]-(R)-PK11195. *Neuroimage* **36**, 28-37.

[20] Fan Z, Aman Y, Ahmed I, Chetelat G, Landeau B, Ray Chaudhuri K, Brooks DJ, Edison P (2015) Influence of microglial activation on neuronal function in Alzheimer's and Parkinson's disease dementia. *Alzheimers Dement* **11**, 608-21.e7.

[21] Kreisl WC, Lyoo CH, McGwier M, Snow J, Jenko KJ, Kimura N, Corona W, Morse CL, Zoghbi SS, Pike VW, McMahon FJ, Turner RS, Innis RB, Biomarkers Consortium PET Radioligand Project Team (2013) *In vivo* radioligand binding to translocator protein correlates with severity of Alzheimer's disease. *Brain* **136**, 2228-2238.

[22] Kreisl WC, Fujita M, Fujimura Y, Kimura N, Jenko KJ, Kannan P, Hong J, Morse CL, Zoghbi SS, Gladding RL, Jacobson S, Oh U, Pike VW, Innis RB (2010) Comparison of [(11)C]-(R)-PK 11195 and [(11)C]PBR28, two radioligands for translocator protein (18 kDa) in human and monkey: Implications for positron emission tomographic imaging of this inflammation biomarker. *Neuroimage* **49**, 2924-2932.

[23] Doens D, Fernandez PL (2014) Microglia receptors and their implications in the response to amyloid beta for Alzheimer's disease pathogenesis. *J Neuroinflammation* **11**, 48.

[24] Imamura K, Hishikawa N, Sawada M, Nagatsu T, Yoshida M, Hashizume Y (2003) Distribution of major histocompatibility complex class II-positive microglia and cytokine profile of Parkinson's disease brains. *Acta Neuropathol* **106**, 518-526.

[25] Pradhan S, Andreasson K (2013) Commentary: Progressive inflammation as a contributing factor to early development of Parkinson's disease. *Exp Neurol* **241**, 148-155.

[26] Chung CY, Koprich JB, Siddiqi H, Isacson O (2009) Dynamic changes in presynaptic and axonal transport proteins combined with striatal neuroinflammation precede dopaminergic neuronal loss in a rat model of AAV alpha-synucleinopathy. *J Neurosci* **29**, 3365-3373.

[27] Tang Y, Le W (2016) Differential roles of M1 and M2 microglia in neurodegenerative diseases. *Mol Neurobiol* **53**, 1181-1194.

[28] Mills CD, Kincaid K, Alt JM, Heilman MJ, Hill AM (2000) M-1/M-2 macrophages and the Th1/Th2 paradigm. *J Immunol* **164**, 6166-6173.

[29] Koenigsknecht-Talboo J, Landreth GE (2005) Microglial phagocytosis induced by fibrillar beta-amyloid and IgGs are differentially regulated by proinflammatory cytokines. *J Neurosci* **25**, 8240-8249.

[30] Cherry JD, Olschowka JA, O'Banion MK (2014) Neuroinflammation and M2 microglia: The good, the bad, and the inflamed. *J Neuroinflammation* **11**, 98.

[31] Heneka MT, Carson MJ, El Khoury J, Landreth GE, Brosseron F, Feinstein DL, Jacobs AH, Wyss-Coray T, Vitorica J, Ransohoff RM, Herrup K, Frautschy SA, Finsen B, Brown GC, Verkhratsky A, Yamanaka K, Koistinaho J, Latz E, Halle A, Petzold GC, Town T, Morgan D, Shinohara ML, Perry VH, Holmes C, Bazan NG, Brooks DJ, Hunot S, Joseph B, Deigendesch N, Garaschuk O, Boddeke E, Dinarello CA, Breitner JC, Cole GM, Golenbock DT, Kummer MP (2015) Neuroinflammation in Alzheimer's disease. *Lancet Neurol* **14**, 388-405.

[32] Amor S, Puentes F, Baker D, van der Valk P (2010) Inflammation in neurodegenerative diseases. *Immunology* **129**, 154-169.

[33] Femminella GD, Rengo G, Pagano G, de Lucia C, Komici K, Parisi V, Cannavo A, Liccardo D, Vigorito C, Filardi PP, Ferrara N, Leosco D (2013) beta-adrenergic receptors and G protein-coupled receptor kinase-2 in Alzheimer's disease: A new paradigm for prognosis and therapy? *J Alzheimers Dis* **34**, 341-347.

[34] Jardanhazi-Kurutz D, Kummer MP, Terwel D, Vogel K, Thiele A, Heneka MT (2011) Distinct adrenergic system changes and neuroinflammation in response to induced locus ceruleus degeneration in APP/PS1 transgenic mice. *Neuroscience* **176**, 396-407.

[35] Femminella GD, Rengo G, Komici K, Iacotucci P, Petraglia L, Pagano G, de Lucia C, Canonico V, Bonaduce D, Leosco D, Ferrara N (2014) Autonomic dysfunction in Alzheimer's disease: Tools for assessment and review of the literature. *J Alzheimers Dis* **42**, 369-377.

[36] Vander Borght T, Minoshima S, Giordani B, Foster NL, Frey KA, Berent S, Albin RL, Koeppe RA, Kuhl DE (1997) Cerebral metabolic differences in Parkinson's and Alzheimer's diseases matched for dementia severity. *J Nucl Med* **38**, 797-802.

[37] Gonzalez-Redondo R, Garcia-Garcia D, Clavero P, Gasca-Salas C, Garcia-Eulate R, Zubieta JL, Arbizu J, Obeso JA, Rodriguez-Oroz MC (2014) Grey matter hypometabolism and atrophy in Parkinson's disease with cognitive impairment: A two-step process. *Brain* **137**, 2356-2367.

[38] Fan Z, Aman Y, Ahmed I, Chetelat G, Landeau B, Ray Chaudhuri K, Brooks DJ, Edison P (2015) Influence of microglial activation on neuronal function in Alzheimer's and Parkinson's disease dementia. *Alzheimers Dement* **11**, 608-621 e607.

[39] Fan Z, Okello AA, Brooks DJ, Edison P (2015) Longitudinal influence of microglial activation and amyloid on neuronal function in Alzheimer's disease. *Brain* **138**(Pt 12), 3685-3698.

[40] Dukart J, Kherif F, Mueller K, Adaszewski S, Schroeter ML, Frackowiak RS, Draganski B, Alzheimer's Disease Neuroimaging I (2013) Generative FDG-PET and MRI model of aging and disease progression in Alzheimer's disease. *PLoS Comput Biol* **9**, e1002987.

[41] Gerhard A, Schwarz J, Myers R, Wise R, Banati RB (2005) Evolution of microglial activation in patients after ischemic stroke: A [11C](R)-PK11195 PET study. *Neuroimage* **24**, 591-595.

[42] Park KW, Kim HS, Cheon SM, Cha JK, Kim SH, Kim JW (2011) Dementia with Lewy bodies versus Alzheimer's disease and Parkinson's disease dementia: A comparison of cognitive profiles. *J Clin Neurol* **7**, 19-24.

[43] Hildebrandt H, Fink F, Kastrup A, Haupts M, Eling P (2013) Cognitive profiles of patients with mild cognitive impairment or dementia in Alzheimer's or Parkinson's disease. *Dement Geriatr Cogn Dis Extra* **3**, 102-112.

[44] Laakso MP, Soininen H, Partanen K, Helkala EL, Hartikainen P, Vainio P, Hallikainen M, Hanninen T, Riekkinen PJ Sr (1995) Volumes of hippocampus, amygdala and frontal lobes in the MRI-based diagnosis of early Alzheimer's disease: Correlation with memory functions. *J Neural Transm Park Dis Dement Sect* **9**, 73-86.

[45] Smith CD, Malcein M, Meurer K, Schmitt FA, Markesbery WR, Pettigrew LC (1999) MRI temporal lobe volume measures and neuropsychologic function in Alzheimer's disease. *J Neuroimaging* **9**, 2-9.

[46] Jucaite A, Cselenyi Z, Arvidsson A, Ahlberg G, Julin P, Varnas K, Stenkrona P, Andersson J, Halldin C, Farde L (2012) Kinetic analysis and test-retest variability of the radioligand [11C](R)-PK11195 binding to TSPO in the human brain - a PET study in control subjects. *EJNMMI Res* **2**, 15.

[47] Lavisse S, Guillermier M, Herard AS, Petit F, Delahaye M, Van Camp N, Ben Haim L, Lebon V, Remy P, Dolle F, Delzescaux T, Bonvento G, Hantraye P, Escartin C (2012) Reactive astrocytes overexpress TSPO and are detected by TSPO positron emission tomography imaging. *J Neurosci* **32**, 10809-10818.

[48] Ji B, Maeda J, Sawada M, Ono M, Okauchi T, Inaji M, Zhang MR, Suzuki K, Ando K, Staufenbiel M, Trojanowski JQ, Lee VM, Higuchi M, Suhara T (2008) Imaging of peripheral benzodiazepine receptor expression as biomarkers of detrimental versus beneficial glial responses in mouse models of Alzheimer's and other CNS pathologies. *J Neurosci* **28**, 12255-12267.

[49] Maeda J, Higuchi M, Inaji M, Ji B, Haneda E, Okauchi T, Zhang MR, Suzuki K, Suhara T (2007) Phase-dependent roles of reactive microglia and astrocytes in nervous system injury as delineated by imaging of peripheral benzodiazepine receptor. *Brain Res* **1157**, 100-111.